Available online at www.sciencedirect.com

ScienceDirect

Energy Procedia 148 (2018) 615–622

Energy Procedia

www.elsevier.com/locate/procedia

73rd Conference of the Italian Thermal Machines Engineering Association (ATI 2018), 12–14 September 2018, Pisa, Italy

Investigation of the Load-Following Capability of CSP Plants

Giovanni Brumana[a], Giuseppe Franchini[a,*], Elisa Ghirardi[a]

[a]*Departement of Engineering and Applied Science, University of Bergamo, Viale Marconi 5, Dalmine 24144 (BG), Italy*

Abstract

The increasing penetration of PV and wind energy in several markets is forcing the power plants (both fossil and renewable) to operate with a high level of flexibility. In this scenario, the load-following capability of CSP power plants can play a fundamental role. The Thermal Energy Storage (TES) system allows exploiting solar energy after sunset and adjusting the power output according to the power demand variability. The paper aims to investigate different CSP plant configurations operating in island-mode to fulfill the power demand of a mid-size town located in the Upington region (South Africa). The power block is based on a steam Rankine cycle with superheated steam temperature 550°C, coupled with a molten salt direct storage system. Two solar fields are compared: Parabolic Trough Collectors (PTCs) and Central Receiver System (CRS). In order to analyze the load-following capability, two different electric loads (with the same annual energy demand of 360 GWh) are considered: the first one is typical of an industrial city, whilst the second one is the power demand pattern of a residential district. A numerical model of the two selected CSP technologies has been developed with the software Trnsys® and the optimization tool GenOpt. The simulation results show that the CSP plant based on CRS exhibits a higher load-following capability: both industrial and residential power demands are met with a lower aperture area and lower investment costs. The PTCs result to be affected by a strong efficiency variation between summer and winter: the load-following capability is good for the residential load profile, whilst is poor for the flat industrial load.

Keywords: CSP power plant; parabolic trough; solar tower.

* Corresponding author. Tel.: +39 035 2052078; fax: +39 035 2052077.
E-mail address: giuseppe.franchini@unibg.it

10.1016/j.egypro.2018.08.149

1. Introduction

A growing market share of renewable energy is ongoing in several countries and is expected to increase further in the next years. Due to the large penetration and their benefic effects [1, 2], the role of the solar power plants is no longer limited to a marginal contribution, and a high dispatchability is becoming a requirement as important as a low price. In spite of a higher LCOE, in the report EIA 2018 [3] Concentrated Solar Power (CSP) plants represent one of the favorite way to produce electricity over photovoltaics especially when the flexibility is a priority as underlined in the study proposed by Gauché et al. in [4].

The availability of an embedded long-term storage system allows supplying thermal energy when the irradiation is low (or fluctuating) and can extend (or shift) the operation of the plant after sunset as reported by Guédez et al. in [5]. The possibility of satisfying the power demand continuously has led the enhancement of CSP plants for standalone grid applications [6]. The predominant TES system for CSP plants is a two-tank molten salt configuration introduced and proven in long-term operation [7, 8] especially for PTC applications.

Nowadays PTCs dominate the installed CSP capacity, though a recent growth in CRS technology has been seen, mainly driven by the ability to achieve higher temperatures [9], raising plant efficiencies and providing lower storage costs. Furthermore, the CRS typically exhibits a flatter thermal collection capability all over the year. However, because of the larger spacing needed by the heliostats, the energy density is lower than the one for the PTC plants.

The electric load pattern represents an important issue in terms of plant operation forecasting [10] and the load-following strategy requires a well-designed thermal energy storage for renewable power plants. The load patterns could differ for variation between daily maximum and minimum and for seasonal fluctuations (summer vs. winter). The patterns of networks with high concentration of residential buildings [11] typically exhibit large daily and seasonal variations, whilst the load curve of industrial districts [12] are usually flat.

Starting from previous works focused on the integration of solarized power plants and electric grids [13] and on the design of CSP plants [14], the present paper aims to investigate the load-following capability of a full-solar power plant. The power systems are assumed to operate in a remote or weakly interconnected grid, and to completely match the electricity demand of a mid-size community. The power block is based on a typical steam Rankine cycle with superheated steam temperature 550°C, coupled with a molten salt mixture direct storage system. Two different solar devices are compared: PTCs with north-south axis orientation and CRS with a field of heliostats reflecting on the tower top. Two typical electric loads, namely industrial and residential, have been considered to estimate pros and cons of the two different CSP plant configurations.

Nomenclature

$A_{SolarField}$	Solar field aperture area (m^2)	Q_{dem}	Thermal power demand (kW)
$C_{###}$	Component unit cost (USD)	T_{amb}	Ambient temperature (K)
DNI	Direct normal irradiance (W/m^2)	Tank	Tank level (%/100)
E_{coll}	Collected heat (MWh)	T_{av}	Average temperature of the collector (K)
E_{dem}	Heat demand (MWh)	T_{sky}	Sky temperature (K)
E_{rad}	Incident solar energy (MWh)	Vol_{tank}	TES volume (m^3)
I_{beam}, I_b	Direct radiation on tilted surface (W/m^2)	V_{wind}	Wind velocity (m/s)
K	Incident angle modifier	ε	Emissivity (-)
$P_{dem,ind}$	Industrial power demand (kW)	η_{el}	Net electric efficiency (%/100)
$P_{dem,res}$	Residential power demand (kW)	η_{opt}	Optical efficiency (-)
Q_{coll}	Collected thermal power (kW)		

2. Design conditions and assumptions

Two typical electric loads, namely industrial and residential, presented in [15, 16] and representing two city districts with different settlements, have been considered to estimate pros and cons of the two different CSP plant

configurations. The two patterns of power demand have the same annual integral value (360 GWh), but different peak values (66 MW vs. 51 MW). The selected CSP plants are supposed to be located in the Upington region (South Africa).

Figure 1 (left part) shows the electric load trends in a typical summer and winter day. The residential load exhibits a large daily variation in the power demand (the minimum is about 50% of the peak), and simultaneously a moderate reduction between summer and winter peak value (58 MW vs. 50 MW): in this case, the load curve is strongly affected by the building air conditioning. The industrial load patterns, on the contrary, show a very limited seasonal variation and a lower distance between maximum (49 MW) and minimum (34 MW).

The performance evaluation of the power block section was analyzed in [14]. The present work focuses on the solar field section, including the Thermal Energy Storage. The right part of Fig. 1 reports the net-to-electric efficiency variation due to the off-design conditions (ambient temperature and partial load) of the power cycle for a typical summer and winter day.

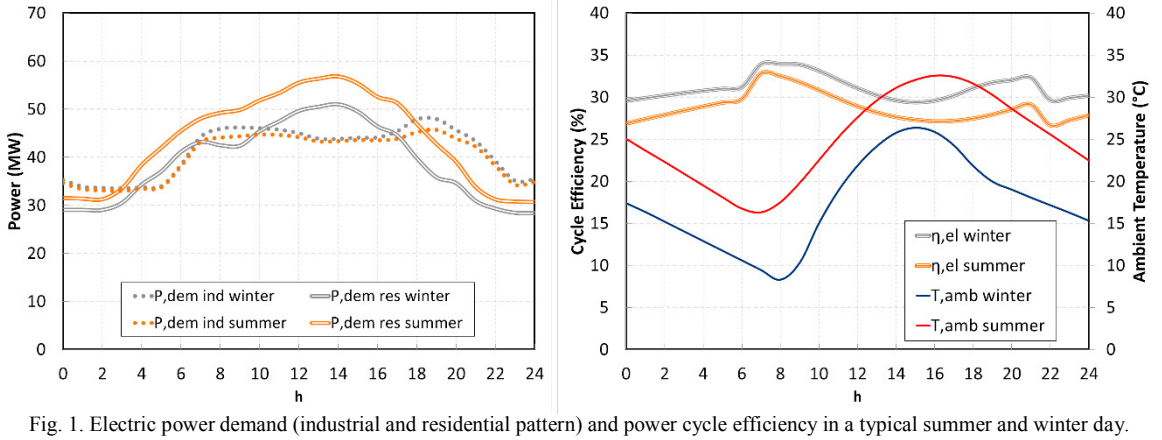

Fig. 1. Electric power demand (industrial and residential pattern) and power cycle efficiency in a typical summer and winter day.

3. Methods and tools

Trnsys® models of the CSP plants have been developed to simulate the plant operation on hourly basis over one-year period. The optimization tool GenOpt was used to determine the optimal aperture area and the optimal storage capacity by minimizing the budget costs.

Meteo data of Upington (solar radiation, ambient temperature and humidity) are taken from the Meteonorm database. The annual average temperature is around 20°C with relatively low oscillations. The relative humidity, responsible of the direct radiation reduction [17], is close to the 40% with slight fluctuations, and encourages the development of CSP plants.

Figure 2 shows the DNI and the ambient temperature for the two representative summer and winter days. The annual DNI is 2720 kWh.

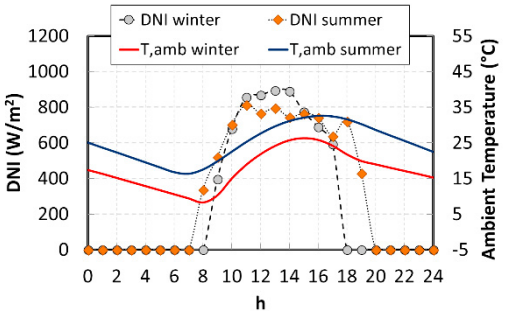

Fig. 2. DNI and ambient temperature in a typical summer and winter day.

3.1. Solar fields

Moving to the solar part, in the CRS the heliostat field is made-up by thousands of mirrors (144 m^2 reflective surface) having a surrounding arrangement and pointing to an external receiver. Many codes and algorithms are devoted to the calculation of the optical losses, including cosine effect, blocking and shading, mirror reflectivity, spillage and atmospheric attenuation [18, 19]. However, the principal parameters affecting the efficiency are the size plant, namely the aperture area of the mirrors and the tower height, and the zenith angle. For the present work, the performance of the heliostat sub-system was simplified to an efficiency map. A complete explanation on the calculation of the heliostat efficiency map is given in [14]. The receiver was considered as a black body absorber and the thermal losses are referred to an area of 1000 m^2.

The solar field based on PTCs is supposed divided in several loops with north-south orientation. Each single collector is 100 m long and 6 m wide, and the loop is made by a series of 8 arrays. The efficiency of the solar collectors was evaluated according to Eq.1 proposed by Moss and Brosseau in [20]. The calculation includes the effective sky temperature for long wave emission and the wind speed to estimate the thermal losses.

$$\eta_{PTC} = \eta_{opt} \cdot K - (A + C \cdot V_{wind}) \cdot \frac{(T_{av} - T_{amb})}{I_b} - \varepsilon \cdot B \cdot \frac{(T_{av}^4 - T_{sky}^4)}{I_b} \qquad \text{(Eq. 1)}$$

The coefficients η_{opt}, A, B and C were computed to fit the thermal efficiency curve of Schott PTR70 receivers under standard conditions [20]. The incident angle modifier K is related to the effect of the non-perpendicularity of solar radiation and it is a function of the incidence angle.

A two-tank Thermal Energy Storage system is considered for each configuration. The heated molten salt mixture is stored in the hot tank and delivered to the steam generator according to the mass flow rate required by the power block. After the heat transfer, the molten salt flow rate is collected in the cold tank.

3.2. Power block

The power block is based on a steam Rankine cycle fed by the solar field without auxiliary fossil-fired heaters. The hot storage tank supplies the molten salt mixture flow rate to the steam generator at 550 °C. The cold storage tank operates at 300 °C. Figure 3 and Table 1 show the power cycle schematic and the main parameters at ISO conditions. A detailed description of the power block is provided in [14].

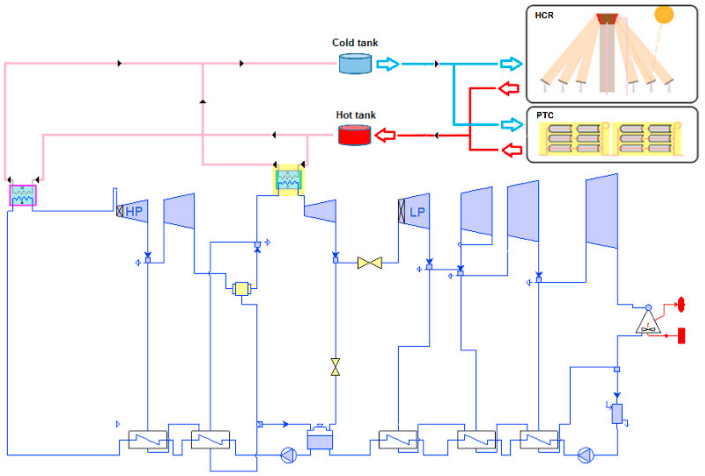

Fig. 3. Power cycle schematic representation.

Table 1. Rankine Cycle parameters at ISO conditions.

	unit	value
Turbine inlet temperature	°C	540
Turbine inlet pressure	bar	100
Steam mass flow at turbine inlet	kg/s	96.8
Reheat temperature	°C	500
Average turbine efficiency	%	86
Extraction pressure	bar	8
Condenser pressure	bar	0.06
SH+EV+EC thermal power	MW	239.1
RH thermal power	MW	35.6
Net electric power	MW	88.9
Thermal efficiency	%	32.3

3.3. Optimization

For each plant configuration, the solar field aperture area and the storage capacity have been determined through an optimization procedure. The Hooke-Jeeves algorithm implemented in the optimization software GenOpt (General Optimization Program) has been selected in order to evaluate the performance of the CSP plants on annual basis. It is based on a direct search pattern method that runs multiple Trnsys simulations, with the aim of minimizing the budget cost function reported in the Eq. 2, by changing the value of the optimization variables. The optimal configurations fulfill hour by hour the power demand with the minimum investment cost. The considered unit costs shown in Table 2 have been estimated according to the economic data reported by the NREL in the System Advisor Model (Version 2017 9.5) [21]. The objective function is the investment cost (C) related to the solar field (troughs for the PTC case; heliostats, tower and receiver for the CRS case): it is calculated according to Eq. 2 (referred to the PTC case). The parameter p is a penalty-cost related to the energy deficit (E_d) and allows rejecting all the plant configurations which cannot meet the power demand.

$$C = A_{SolarField} \cdot C_{PTC} + Vol_{tank} \cdot C_{tank} + p \cdot E_d \qquad \text{(Eq. 2)}$$

4. Simulation results

The results of the optimization procedure are summarized in Table 3, for each CSP technology and each load profile pattern. The plant configurations based on CRS need a lower aperture area (-28% for the industrial load, -10.5% for the residential load, respectively). The capacity of the TES system is larger in the residential case for both PTC and CRS: this is related to the higher fluctuation of the residential power demand. With regard to the global cost, the CRS appears more cost effective for all cases (-11.7% industrial, -4.2% residential). More in detail, the industrial case shows a large difference between PTC and CRS in terms of solar aperture area, and the solar field is responsible for more than 80% of the global cost. The residential case, on the contrary, exhibits a similar solar field cost (354 vs. 349 Mio USD), and the larger cost of the PTC configuration is mainly due to the higher storage capacity.

Table 2. Budget costs.

	unit	value
C_{PTC}	USD/m^2	250
C_{CRS}	USD/m^2	275
C_{tank}	USD/m^3	4850

Table 3. Optimal design parameters.

	unit	PTC	CRS
Industrial Case			
$A_{SolarField}$	m^2	1,600,000	1,152,000
Vol_{tank}	m^3	30,000	32,000
Global Cost	10^6 USD	545.5	481.7
Residential Case			
$A_{SolarField}$	m^2	1,416,000	1,270,000
Vol_{tank}	m^3	38,000	34,500
Global Cost	10^6 USD	538.3	515.8

Moving to the transient simulations, firstly the daily simulation results related to two representative summer and winter days are presented. Then, the monthly and annual simulation outputs will be shown and discussed.

4.1. Daily simulation results

Figure 4 shows the solar-to-thermal efficiency of the two investigated solar fields. It is clear that PTC and CRS perform differently. PTC efficiency dramatically decays in winter days because of the cosine effect and lower ambient temperatures. The solar field efficiency for CRS configuration is slightly lower in summer (59% vs. 66% in the central hours of the day), but significantly higher in winter (56% vs. 31%). This is due to the benefits of the 2-axis tracking system.

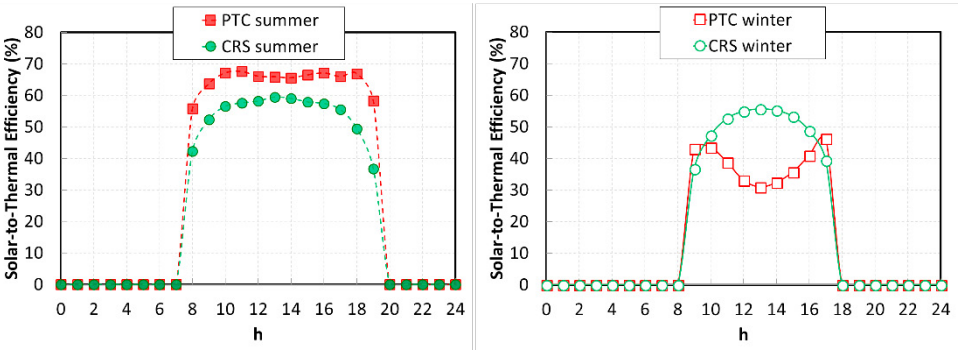

Fig. 4. Solar-to-thermal efficiency (%) in a typical summer and winter day.

Figure 5 shows the hourly results for each plant configuration and load pattern. Plots report the collected heat (Q_{coll}) and the instantaneous heat demand required by the power block (Q_{dem}), for a representative summer (full symbols) and winter day (hollow symbols). The hot storage tank level is also reported.

In the industrial load case, the PTC solar field appears oversized in summer, when the peak value of the collected heat is 880 MW, whilst the maximum heat demand is 150 MW. This is due to the low performance in winter, when the PTC efficiency almost halves. Therefore, for many hours per day a fraction of the troughs must be defocused, since the hot storage tank is at the maximum capacity. On the contrary, the CRS plant configuration exhibits similar performance in summer and winter, as documented by the efficiency curves reported in Figure 4. The lower aperture area and the more constant efficiency pattern allows minimizing the heliostat defocusing, as confirmed by the limited number of hours with full hot tank.

Moving to the residential load case, the solar radiation profile and the power demand pattern are more in-phase. For this reason, the PTC over-sizing is reduced (peak production 750 MW vs. peak demand 200 MW). Nevertheless, a significant defocusing takes place in summer. The advantages of the CRS configurations documented in the industrial case appear less evident in the residential case. The bell-shaped profile of the power demand does not fit much the flat CRS efficiency curve. This reduces the competitiveness of CRS on PTCs.

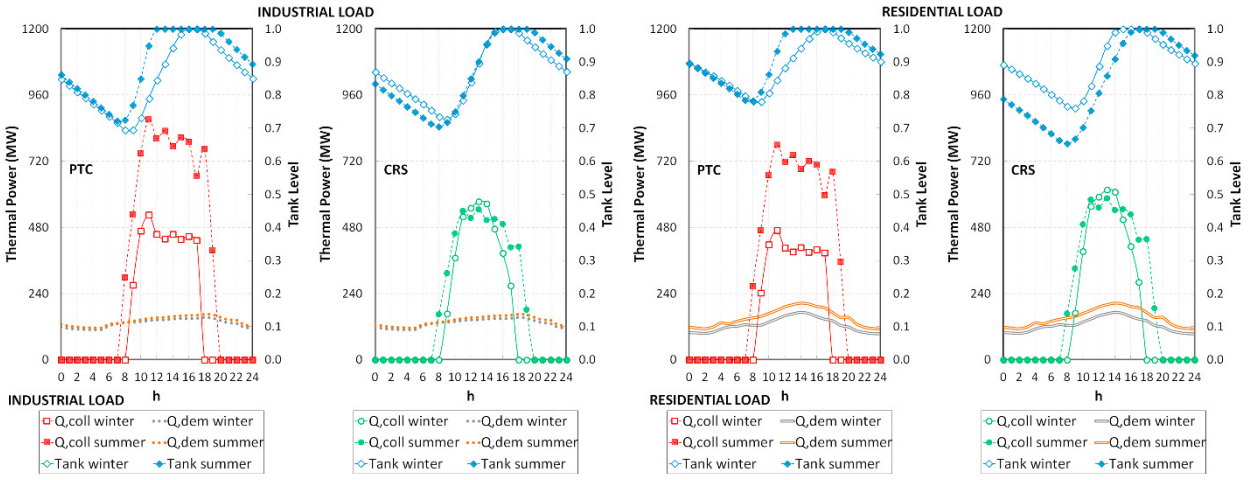

Fig. 5. Solar field daily simulation results.

4.2. Monthly and yearly performance

Figures 6 and 7 show the monthly energy amounts, namely the available solar energy (E_{rad}), the collected heat (E_{coll}) and the power block thermal input demand (E_{dem}), for the two load profiles. A different behavior can be noticed

depending on the solar field. Looking at the PTC performance, in summer the heat collection strongly exceeds (even up to 150% from October to March) the heat demand. In winter, the energy collected daytime is just enough to drive the power block and the limited energy surplus is sent to the storage. For these reasons, the design requires to oversize the aperture area and many troughs in summer must be defocused.

The CRS monthly thermal production is fairly stable throughout the year and slightly larger than the heat energy demand. In the residential case, the thermal dumping is slightly higher compared to the industrial case, mainly in winter when the power demand has its minimum.

In order to globally evaluate the performance of the investigated configurations, the annual energy balance is reported in Table 4. It can be seen that the CSP plants based on CRS require a lower amount of solar energy (consequently, a lower aperture area) to meet both load profiles. This advantage is more noticeable in the industrial load case. The surplus of collected energy (requiring the defocusing of a fraction of solar devices) is higher for the plant configurations based on parabolic troughs.

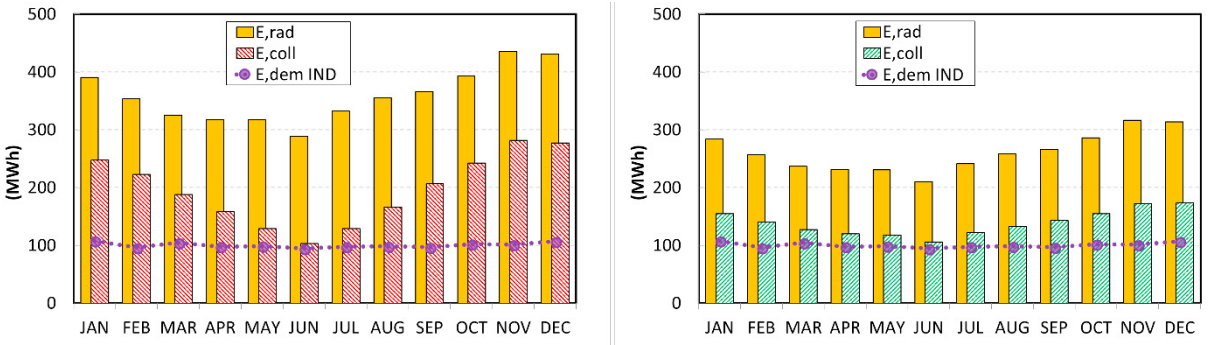

Fig. 6. Monthly simulation results for PTCs (left) and CRS (right) with industrial load.

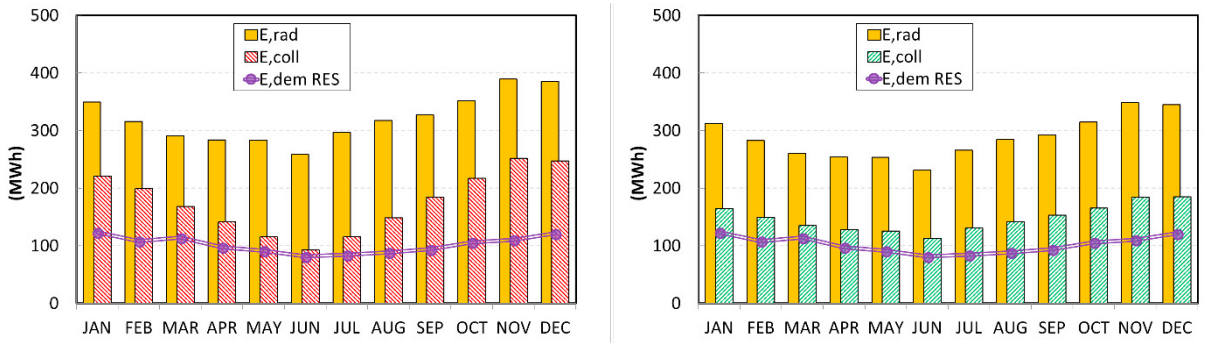

Fig. 7. Monthly simulation results for PTCs (left) and CRS (right) with residential load

Table 4. Annual energy balance.

		Industrial		Residential	
	unit	PTC	CRS	PTC	CRS
Solar energy	GWh	4304.61	3130.6	3848.06	3443.69
Collected heat	GWh	2350.06	1614.3	2100.81	1775.74
Heat demand	GWh	1202.5		1220.5	
Energy surplus (defocusing)	%	47.94	25.5	40.70	31.26

5. Conclusion

The load following capability of full-solar CSP plants has been assessed. The investigation has been carried out for two different concentrated solar devices (PTCs and CRS) and for two power demand patterns, namely industrial and

residential load. An optimization procedure has been developed in order to find out the optimal aperture area and the optimal storage capacity. For both electric load patterns, the CRS plant configuration allows fulfilling the power demand by minimizing the investment costs. Thanks to a flatter efficiency curve, due to the 2-axis tracking system, the solar tower plant shows a better load-following capability: this behavior is emphasized with the industrial load, which has small seasonal variations.

The CSP plants based on parabolic troughs, on the contrary, need an over-sizing of the solar field area, because of the low optical efficiency in winter. This leads to a large surplus of collected heat in summer, thus requiring the defocusing of several troughs. This issue is particularly evident with the industrial load pattern. The residential load profile is more in-phase with the PTC efficiency curve: this makes the investment costs comparable with the CRS plant configuration (+4%).

For all the considered cases, the role of a large TES system is fundamental to operate the CSP plant according to a load following strategy.

References

[1] Forrester, Jon. "The value of CSP with thermal energy storage in providing grid stability." Energy Procedia 49 (2014): 1632-1641.
[2] Denholm, Paul, and Mark Mehos “Enabling Greater Penetration of Solar Power via the Use of CSP with Thermal Energy Storage” Technical Report NREL/TP -6A20-52978 November 2011
[3] EIA, US. "Levelized cost and levelized avoided cost of new generation resources in the annual energy outlook 2016." EIA. [Online]. Available: http://www. eia. gov/outlooks/aeo/pdf/electricity_generation.pdf.
[4] Gauché, Paul, Justine Rudman Mbalenhle Mabaso, Willem A. Landman, Theodor W.von Backström, and Alan C. Brent. "System value and progress of CSP." Solar Energy 152 (2017): 106-139.
[5] Guédez, Rafael, James Spelling, and Björn Laumert. "Thermoeconomic optimization of solar thermal power plants with storage in high-penetration renewable electricity markets." 2013 ISES Solar World Congress, SWC 2013; Cancun; Mexico; 3 November 2013 through 7 November 2013. Vol. 57. 2013.
[6] Iaquaniello, Gaetano, William Montanari, and Annarita Salladini. "Standalone CSP-DG system for electrification of remote areas and desalinated water supply." Solar Energy 157 (2017): 1056-1063
[7] Herrmann, Ulf, Bruce Kelly, and Henry Price. "Two-tank molten salt storage for parabolic trough solar power plants." Energy 29.5-6 (2004): 883-893.
[8] Kearney, David, Ulf Herrmann, Paul Nava, Bruce D. Kelly, Rod Mahoney, James E. Pacheco, Robert Cable, N. Potrovitza, Daniel Blake, and Henry Price. "Assessment of a molten salt heat transfer fluid in a parabolic trough solar field." Journal of solar energy engineering 125.2 (2003): 170-176.
[9] Ho, Clifford K. "Advances in central receivers for concentrating solar applications." Solar Energy 152 (2017): 38-56.
[10] Shepero, Mahmoud, Dennis van der Meer, Joakim Munkhammar, and Joakim Widén. "Residential probabilistic load forecasting: A method using Gaussian process designed for electric load data." Applied Energy 218 (2018): 159-172.
[11] Grandjean, Arnaud, Jérôme Adnot, and Guillaume Binet. "A review and an analysis of the residential electric load curve models." Renewable and Sustainable Energy Reviews 16.9 (2012): 6539-6565.
[12] Vaghefi, Abolfazl, Farbod Farzan, and Jafari A. Mohsen. "Modeling industrial loads in non-residential buildings." Applied Energy 158 (2015): 378-389.
[13] Perdichizzi, Antonio, Giovanna Barigozzi, Giuseppe Franchini, and Silvia Ravelli. "Peak shaving strategy through a solar combined cooling and power system in remote hot climate areas." Applied Energy 143 (2015): 154-163.
[14] Ravelli, Silvia, Giuseppe Franchini, and Antonio Perdichizzi. "Comparison of different CSP technologies for combined power and cooling production." Renewable Energy 121 (2018): 712-721.
[15] Van Deventer, A. "South African power system status overview." 64th Association of Municipal Electricity Convention 2014. 2014.
[16] Franchini, Giuseppe., Antonio Perdichizzi, and Silvia Ravelli. "Performance prediction of solarized CC power plants operating in a load-following strategy." Power-Gen Africa 2016. (2016).
[17] Hanrieder, Natalie, Manajit Sengupta, Yu Xie, Stefan Wilbert, and Robert Pitz-Paal. "Modeling beam attenuation in solar tower plants using common DNI measurements." Solar Energy 129 (2016): 244-255.
[18] Cruz, Nicolas C., Juana L. Redondo, Manuel Berenguel, José D. Álvarez, and Pilar. M. Ortigosa. "Review of software for optical analyzing and optimizing heliostat fields." Renewable and Sustainable Energy Reviews 72 (2017): 1001-1018.
[19] Garcia-Barberena, Javier, Amaia Mutuberria Larrayoz, Marcelino Sánchez, and Ana Bernardos. "State-of-the-art of heliostat field layout algorithms and their comparison." Energy Procedia 93 (2016): 31-38.
[20] T. Moss, D. Brosseau, Testing Capabilities NSTTF (AZTRAK) Rotating Platform, Sandia National laboratories, New Mexico, 2007.
[21] Nate Blair, Aron P. Dobos, Janine Freeman, Ty Neises, Michael Wagner, Tom Ferguson, Paul Gilman, and Steven Janzou. “System Advisor Model, SAM 2014.1.14 e General Description” Technical Report NREL/TP-6A20e61019 February 2014.